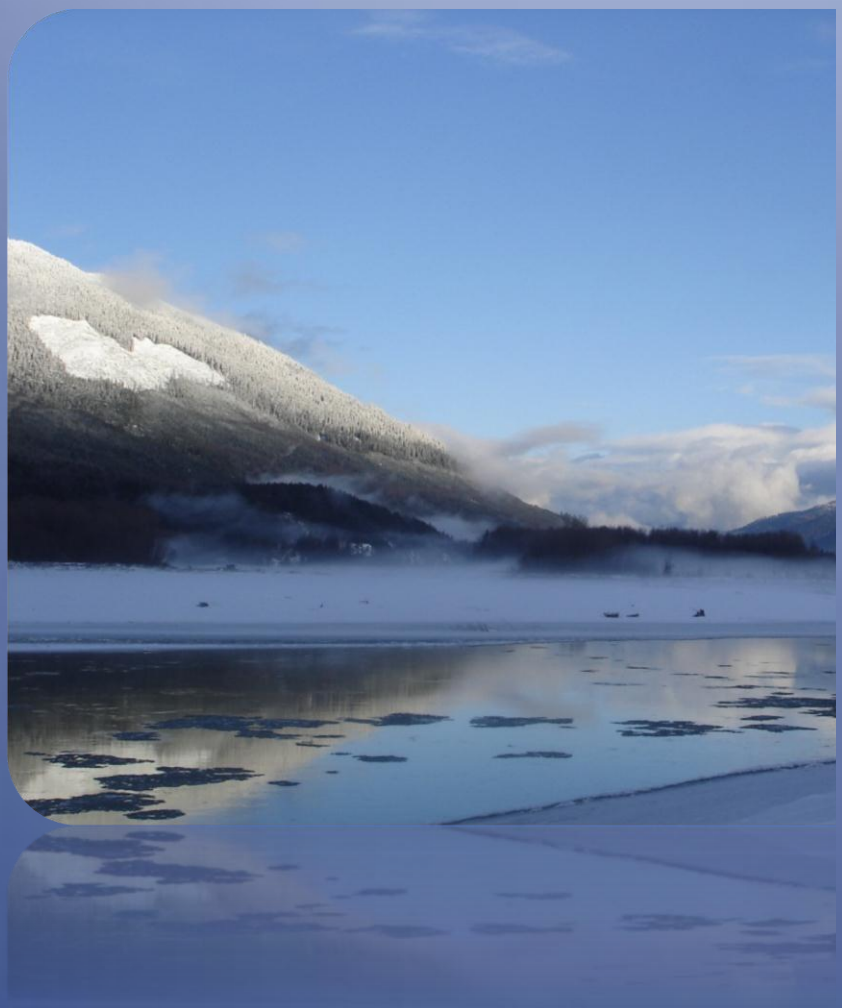

Chapter 5: Climate Change Projections for the Northwest Skeena

Joe Melton, Jed Kaplan, Don Robinson

Chapter 5: Climate Change Projections for the Northwest Skeena

5.1 Emissions and Climate Change Scenarios

There is a lot of uncertainty around the extent of climate change in the future especially because of the challenge of estimating the level of greenhouse gasses (GHGs) that will be emitted. Greenhouse gas emissions are dependent on a number of factors, including global population, demographic trends, socio-economic conditions and policy, global energy policy, and technology development. The Inter-governmental Panel of Climate Change (IPCC), has developed four different storylines (Figure 5.1), that represent possible different futures and their associated projections for GHG emissions (Nakicenovic, et al, 2000).

Within the storylines are families of scenarios that result in different long-term emissions and climate projections. A number of models have been used to project the range of impacts that these emission scenarios could have. The outputs from these models can then be downscaled to specific regions in order to inform adaptive actions, mitigation, and to assess impacts on specific resources to help policy-makers, planners, and other stakeholders better understand the range of future conditions to which they may have to adapt. Key characteristics of the four families can be found in Table 5.1.

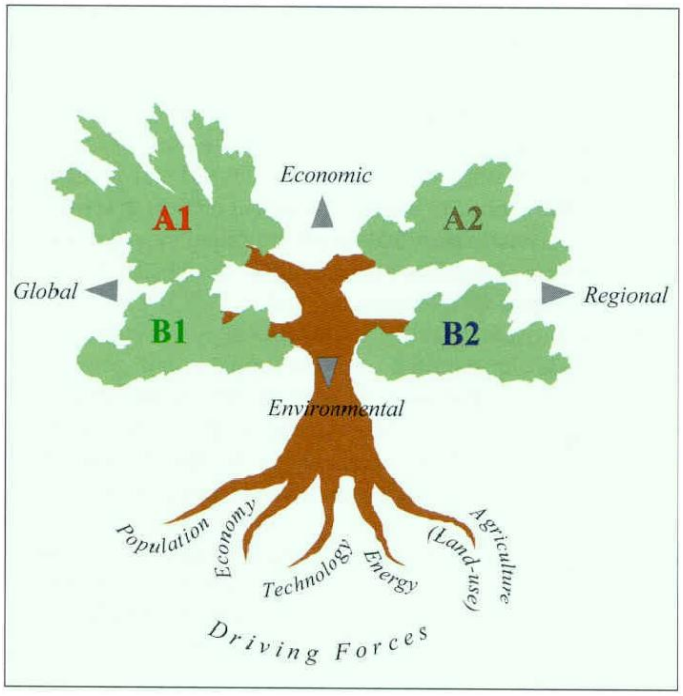

Figure 5.1 This diagram represents the different families developed by the IPCC special report on emissions scenarios (IPCC, 2000). The branches represent characteristics of each family, while the roots represent a number of factors influencing future emissions scenarios. (Cohen & Wadell, 2009)

5.2 Climate Projections for the Skeena Region

The Skeena region was modeled using a dynamic global vegetation model called LPJ-GUESS at a grid resolution of 30 arc seconds (about 1 km^2). Historical climate data was used as input to the model for the years 1906 to 2006. Future greenhouse gas (GHG) emissions scenarios/climate model outputs from the Inter-governmental Panel on Climate Change (IPCC) 4^{th} Assessment (Meehl et al., 2007) were selected following the recommendations of Spittlehouse and Murdock (2010) to cover a wide possible

range in future climate conditions. From the six emission scenarios listed in Table 5.1, three emission scenarios and climate model outputs were selected and are listed in Table 5.2.

Table 5.1: This table highlights socio-economic, population, energy and technology trends of the 6 different emissions scenarios released in 2000 by the IPCC (Adapted from Nakicenovic, et al, 2000)

A1		• Rapid economic growth • Global population increase and peak mid-century at 8.7 billion, falling to around 7 billion by 2100 • Rapid introduction of new, resource efficient technologies
	A1FI	• Energy is fossil fuel intensive
	A1B	• Energy development is balanced
	A1T	• Predominantly non-fossil fuel
A2		• Heterogeneous world with emphasis on self-reliance • Increasing global population to 15 billion by 2100 • Fragmented per capita economic growth • Slow technological growth and dissemination
B1		• Global solutions to economic, social and environmental sustainability. • Improved equity in population reaching peak at mid-century, similar to A1 • Shift in economic structures toward service and information • Decrease in material intensity • Introduction of clean and resource efficient technologies
B2		• Local solutions to economic, social and environmental sustainability. • Continuous population growth at slower rate than A2 to 10.4 billion by 2100 • Focus on environmental protection and social equity at the local / regional scale • Slower but more diverse dissemination of technology than A1 or B1

Table 5.2: Selected emissions scenarios/climate model output for the SW Skeena Region future vegetation simulations. Emissions scenarios follow those defined in the IPCC Special Report on Emissions Scenarios (Nakicenovic et al., 2000) and are the minimum subset suggested by Spittlehouse and Murdock (2010) to adequately cover the possible future climate space for British Columbia. The climate models listed are the U.K. Met Office Hadley Centre GEM (UKMO-HADGEM) and CM3 (UKMO-HADCM3) models as well as the Canadian Centre for Climate Modelling and Analysis CGCM3 (CCCMA-CGCM3) model. Please note: The general climate descriptions are described here relative to each other differentiated to historical climate for the region.

Emissions scenario	Climate model	Climate model run number	General relative description	Short name
A1B	UKMO-HADGEM	1	Warmest & wet	HADGEM-A1B
A2	CCCMA-CGCM3	4	Warmer & wetter	CGCM3-A2
B1	UKMO-HADCM3	1	Warm & wetter	HADCM3-B1

Global CO_2 levels from observational databases were used as input to LPJ-GUESS for the historical period. Future CO_2 concentrations follow those used to generate the climate model outputs. The present trajectory of global CO_2 closely follows these three scenarios with present CO_2 below the A1B emissions scenario, but above both the A2 and B1 emissions scenarios (Manning et al., 2010).

5.2.1 Mean Annual Temperature

The three climate scenarios used (HADGEM-A1B, CGCM3-A2, and HADCM3-B1) all show an increase in mean annual temperature for the study region (Fig 5.2 and Table 5.3). The scenario showing the maximal increase is HADGEM-A1B with an increase of almost 5°C for the 2080s compared to the 1961 – 1990 climate normal. The temperature increase for scenario HADCM3-B1 is relatively weak (2.3°C).

Table 5.3: Summary of projected climate changes to the study region by time period and emissions/model scenario. The relative terminology between emissions/model scenarios is, as introduced in Table 2, warmest & wet (HADGEM-A1B), warmer & wetter (CGCM3-A2), and warm & wetter (HADCM3-B1).

Time period	Emissions / Model Scenario	Mean temperature change relative to the 1961 – 1990 annual mean (°C)	Mean precipitation change relative to the 1961 – 1990 annual total (%)
2020s (2010-2039)	CGCM3-A2	+2.0	+11.5
	HADCM3-B1	+1.0	+10.4
	HADGEM-A1B	+1.4	+0.3
2050s (2040-2069)	CGCM3-A2	+2.7	+16.0
	HADCM3-B1	+1.7	+17.2
	HADGEM-A1B	+3.3	+3.6
2080s (2070-2099)	CGCM3-A2	+4.1	+23.3
	HADCM3-B1	+2.3	+22.4
	HADGEM-A1B	+4.9	+7.0

5.2.2 Seasonal Maximum Monthly Temperature

Downscaled seasonal maximum monthly temperature is presently only available for a separate climate model output than those used to drive the LPJ-GUESS suite of simulations and only for one emissions scenario. The available downscaled climate model output is from the CGCM2 model (this is an earlier generation of the CGCM model used in the bulk of this study) for the A2 emissions scenario (Flato et al., 2000). This climate model output was downscaled with the ClimateBC software (Wang et al., 2006)

The 2080s (2070-2099) winter maximal monthly temperatures, relative to the 1961-1990 climate normal, show an increase of between 3.4° to 4.1°C (Fig 5.3). Spring has the largest increase across all seasons with a projected increase of between 4.0° and 5.3°C (Fig 5.4). Estimated summer maximal monthly temperatures show a relatively constant increase of about 3.4°C (Fig 5.5). Autumn has the smallest projected temperature increase of about 3.0°C (Fig 5.6). All seasons except summer show a

larger projected temperature increase in the eastern regions of the study area due to the moderating influence of the ocean on the surrounding climate in the coastal regions.

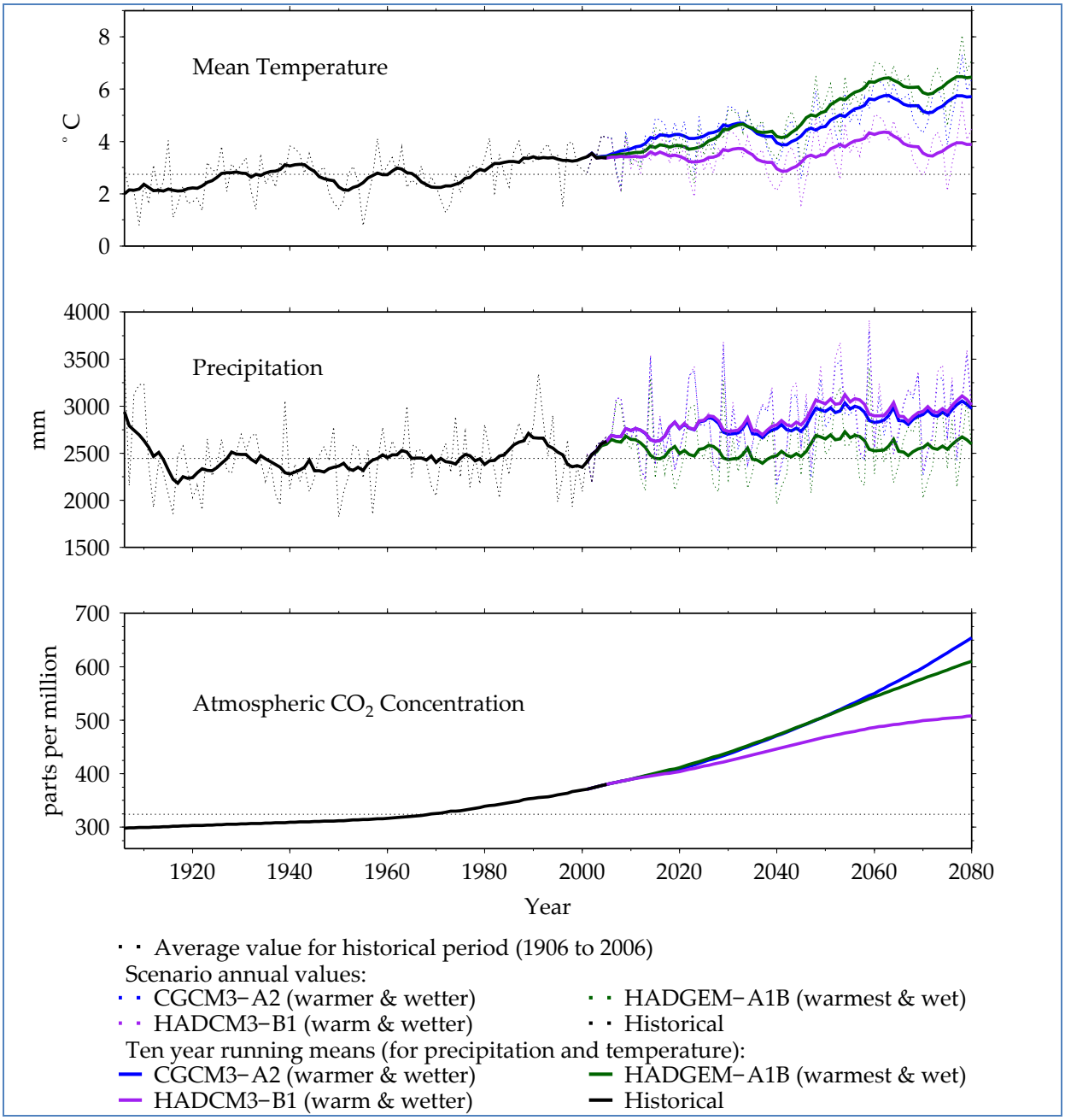

Figure 5.2: Mean annual temperature, total precipitation and atmospheric CO2 concentration from 1906 to 2080 for the study region and each emissions / model scenario.

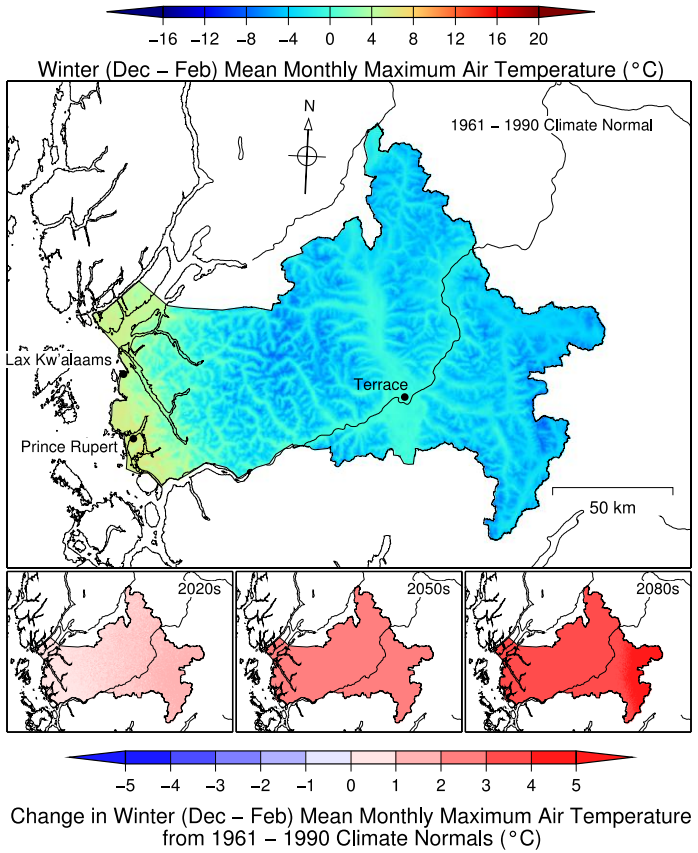

Figure 5.3: Winter mean monthly maximum air temperature and future anomalies. Anomalies are calculated by subtracting the 1961 – 1990 climate normal (upper figure) from a mean climate year created by averaging over 30 years centering on the 2020s (2010-2039), 2050s (2040-2069) and 2080s (2070-2099). The anomaly calculation results in the lower series of maps showing how much temperature change is projected for each future time period relative to present day (1961 – 1990 climate normal). Note: this climate was generated by the CGCM2 model for scenario A2 (Flato, et al., 2000).

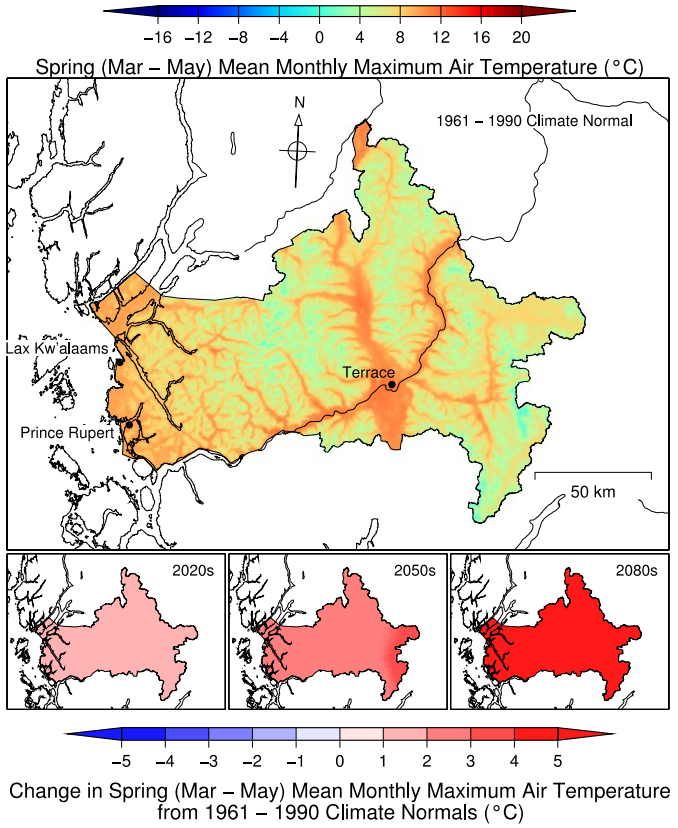

Figure 5.4: Spring mean monthly maximum air temperature and future anomalies. Anomalies are calculated by subtracting the 1961 – 1990 climate normal (upper figure) from a mean climate year created by averaging over 30 years centering on the 2020s (2010-2039), 2050s (2040-2069) and 2080s (2070-2099). The anomaly calculation results in the lower series of maps showing how much temperature change is projected for each future time period relative to present day (1961 – 1990 climate normal). Note this climate was generated by the CGCM2 model for scenario A2 (Flato, et al., 2000)

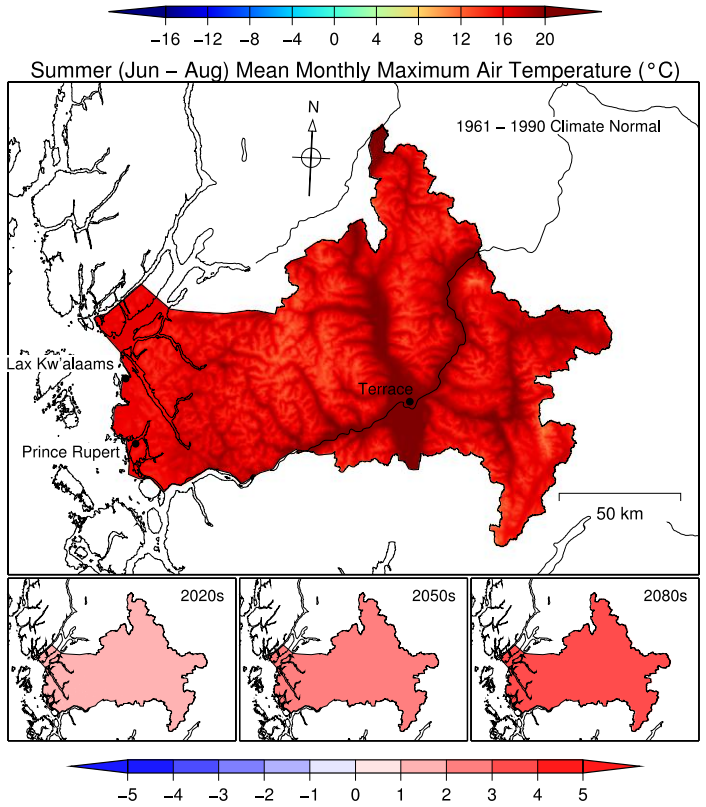

Figure 5.5: Summer mean monthly maximum air temperature and future anomalies. Anomalies are calculated by subtracting the 1961 – 1990 climate normal (upper figure) from a mean climate year created by averaging over 30 years centering on the 2020s (2010-2039), 2050s (2040-2069) and 2080s (2070-2099). The anomaly calculation results in the lower series of maps showing how much temperature change is projected for each future time period relative to present day (1961 – 1990 climate normal). Note this climate was generated by the CGCM2 model for scenario A2 (Flato, et al., 2000)

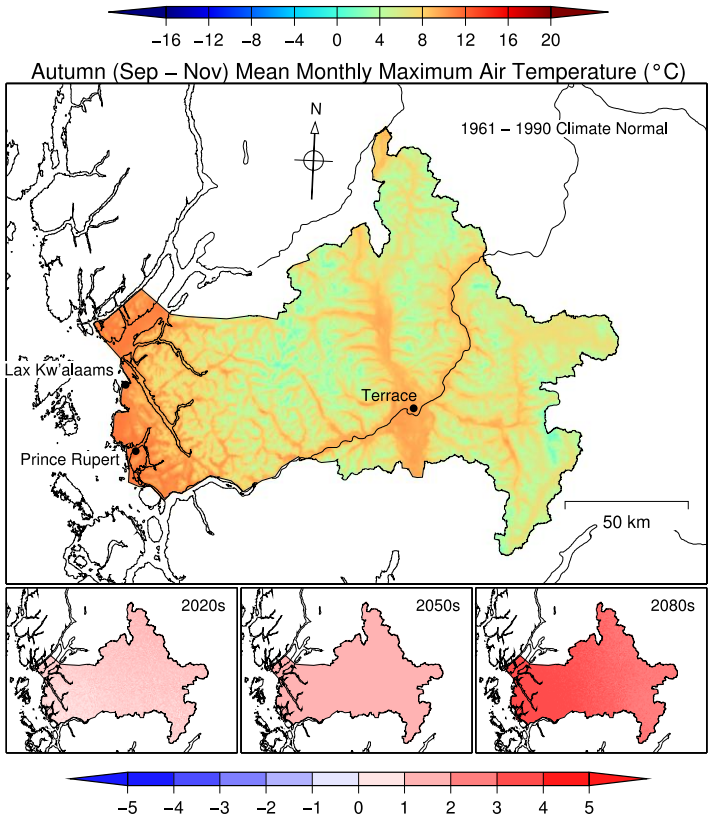

Figure 5.6: Autumn mean monthly maximum air temperature and future anomalies. Anomalies are calculated by subtracting the 1961 – 1990 climate normal (upper figure) from a mean climate year created by averaging over 30 years centering on the 2020s (2010-2039), 2050s (2040-2069) and 2080s (2070-2099). The anomaly calculation results in the lower series of maps showing how much temperature change is projected for each future time period relative to present day (1961 – 1990 climate normal). Note this climate was generated by the CGCM2 model for scenario A2 (Flato, et al., 2000).

5.2.3 Seasonal Minimum Monthly Temperature

The available downscaled climate model output is from the same model output as seasonal maximal monthly temperature (Section 2.1.2; CGCM2 model) for the A2 emissions scenario (Flato, et al., 2000) downscaled with the ClimateBC software (Wang, et al., 2006).

For the 2080s (2070-2099) relative to the 1961-1990 climate normal, minimum monthly temperatures are projected to increase between 3.6° and 4.9°C in winter (Fig 5. 7), between 4° and 5.2° C in spring (Fig 5.8), about 3.5°C in summer (Fig 5.9), and about 3.0°C for autumn (Fig 5.10). There is a gradient in the winter and spring with stronger projected temperature increases in the northern areas of the study region. This coincides with a polar amplification of the climate warming. Polar amplification describes the pattern where the largest increases in global temperature are within the polar regions with lesser increases moving towards the equator. The summer and autumn projected increases have a slight gradient with larger temperature increases in the eastern parts of the study region. These increases in minimum monthly temperature generally show a more rapid increase than the maximum monthly temperature.

5.2.4 Seasonal Mean Monthly Temperature

Seasonal mean monthly temperature is available for all three future climate scenarios. Winter mean monthly temperatures are projected to increase most strongly in the CGCM3-A2 scenario (increase of 4.3° to 5.2°C for the 2080s, as compared to the 1961 – 1990 climate normal) with a relatively mild increase for the HADCM3-B1 scenario (even a slight cooling in the 2020s) (Fig 5.11). The projected increase is strongest in the northern parts of the study region consistent with polar amplification of climate warming (Meehl, et al., 2007). The projected winter monthly mean temperature increases are the most inconsistent between the different scenarios of all seasons.

The projected spring mean monthly temperature increase is consistently strong across all climate scenarios (Fig 5.12). The increase in mean temperature is between 6.4° to 8.9°C for the HADGEM-A1B scenario with the warming strongest in the eastern part of the study region. The coastal regions are moderated by their proximity to the ocean, which warms slowly due to its high heat capacity and the ability of currents to bring in cooler water.

Projected summer increases in mean monthly temperature are relatively consistent across all scenarios with the strongest increase in the HADGEM-A1B scenario (Fig 5.13). The 2080s mean monthly temperature increase from the 1961-1990 climate normal for the HADGEM-A1B scenario could be between 6.5° to 8.7°C with higher increases in the northern and eastern parts of the study region.

Autumn mean monthly temperature cooling is projected to occur across all climate scenarios (Fig 5.14). This consistent cooling pattern decreases slightly from the 2020s to the 2080s with the HADGEM-A1B showing some slight coastal warming. The largest cooling is projected in the 2020s for the HADGEM-A1B and HADCM3-B1 scenarios with a temperature decrease of between 4.4° and 1.2°C. The least cooling occurs in the coastal regions.

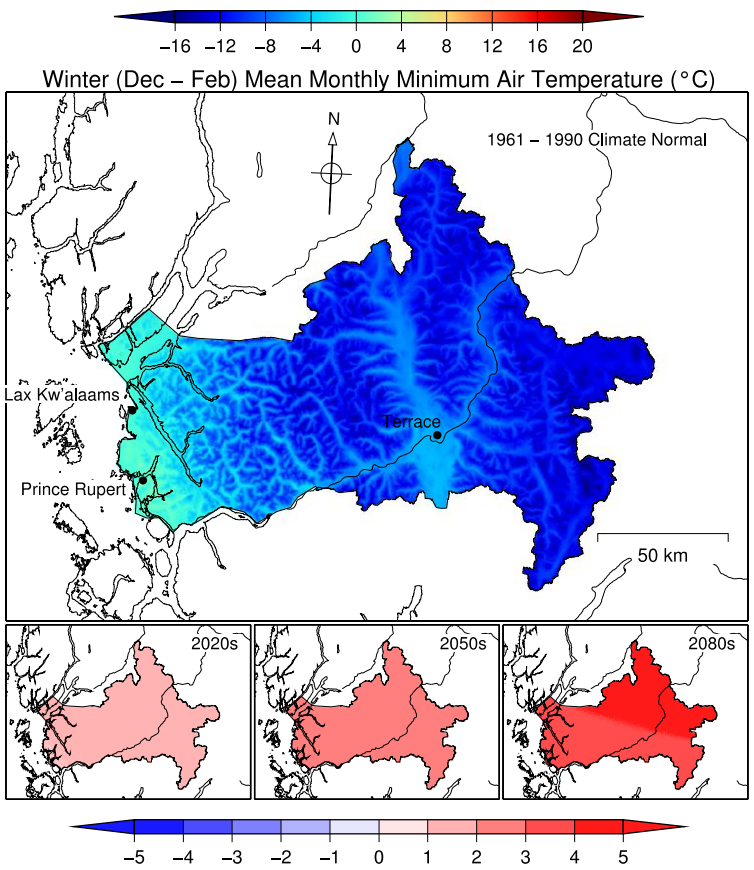

Figure 5.7: Winter mean monthly minimum air temperature and future anomalies. Anomalies are calculated by subtracting the 1961 – 1990 climate normal (upper figure) from a mean climate year created by averaging over 30 years centering on the 2020s (2010-2039), 2050s (2040-2069) and 2080s (2070-2099). The anomaly calculation results in the lower series of maps showing how much temperature change is projected for each future time period relative to present day (1961 – 1990 climate normal). Note this climate was generated by the CGCM2 model for scenario A2 (Flato, et al., 2000)

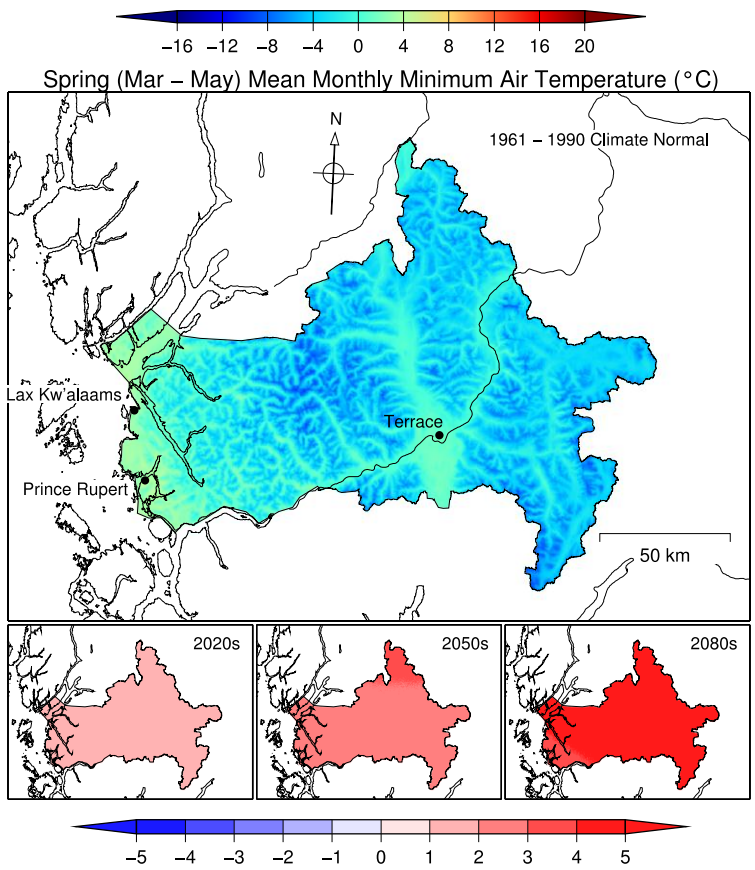

Figure 5.8: Spring mean monthly minimum air temperature and future anomalies. Anomalies are calculated by subtracting the 1961 – 1990 climate normal (upper figure) from a mean climate year created by averaging over 30 years centering on the 2020s (2010-2039), 2050s (2040-2069) and 2080s (2070-2099). The anomaly calculation results in the lower series of maps showing how much temperature change is projected for each future time period relative to present day (1961 – 1990 climate normal). Note this climate was generated by the CGCM2 model for scenario A2 (Flato, et al., 2000)

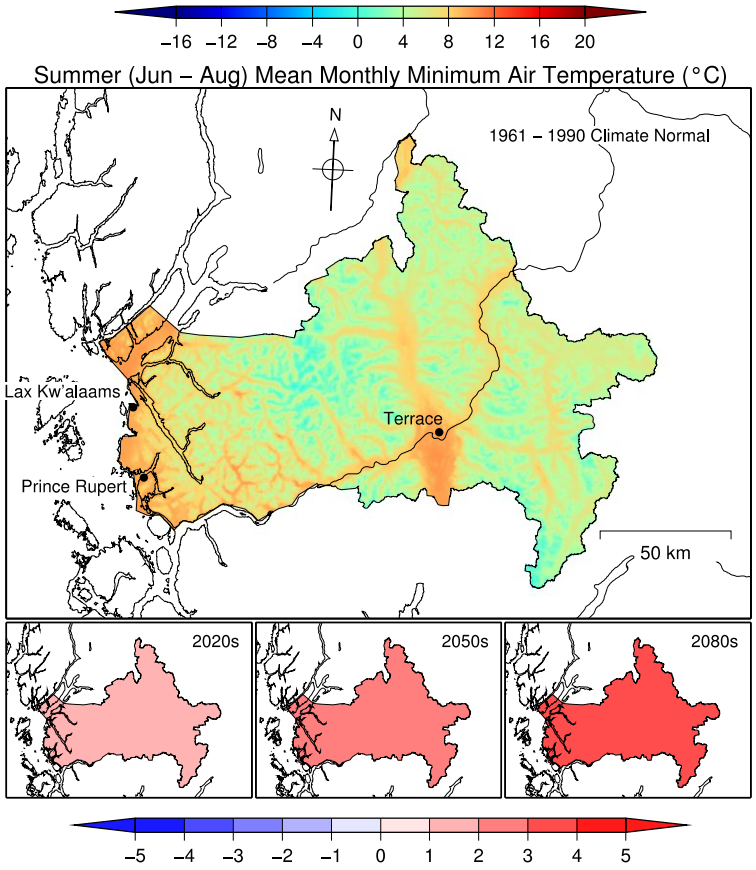

Figure 5.9: Summer mean monthly minimum air temperature and future anomalies. Anomalies are calculated by subtracting the 1961 – 1990 climate normal (upper figure) from a mean climate year created by averaging over 30 years centering on the 2020s (2010-2039), 2050s (2040-2069) and 2080s (2070-2099). The anomaly calculation results in the lower series of maps showing how much temperature change is projected for each future time period relative to present day (1961 – 1990 climate normal). Note this climate was generated by the CGCM2 model for scenario A2 (Flato, et al., 2000).

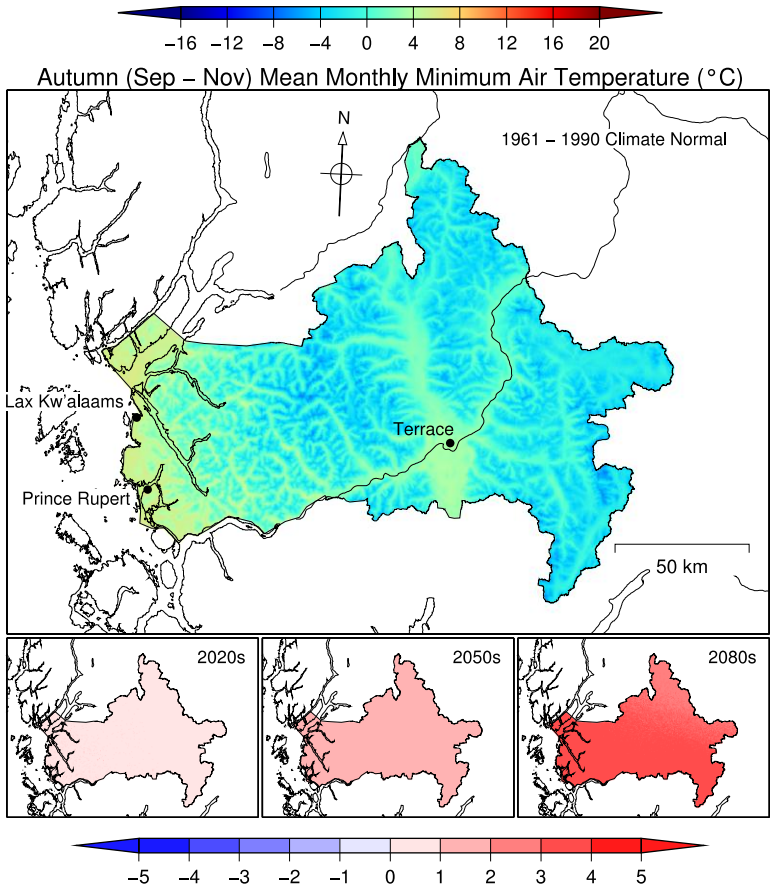

Figure 1.10: Autumn mean monthly minimum air temperature and future anomalies. Anomalies are calculated by subtracting the 1961 – 1990 climate normal (upper figure) from a mean climate year created by averaging over 30 years centering on the 2020s (2010-2039), 2050s (2040-2069) and 2080s (2070-2099). The anomaly calculation results in the lower series of maps showing how much temperature change is projected for each future time period relative to present day (1961 – 1990 climate normal). Note this climate was generated by the CGCM2 model for scenario A2 (Flato, et al., 2000).

5.2.5 Annual Precipitation

Annual precipitation is projected to increase over 20% from the historical 1906 - 2006 mean by the year 2080 for the HADCM3-B1 and CGCM3-A2 scenarios (Fig 5.2 and Table 5.3). The HADGEM-A1B scenario shows only a slight increase from the end of the historical period to 2080 (ca. 7%).

5.2.6 Seasonal Precipitation

The three climate scenarios show an inconsistent change in winter precipitation with an increase for scenarios CGCM3-A2 and HADCM3-B1 and a general decrease for HADGEM-A1B (Fig 5.15). The disparity between the climate scenarios increases into the future with the 2080s showing a large difference (>15%) between the CGCM3-A2 and HADGEM-A1B scenarios in the interior parts of the study region.

Projected spring precipitation patterns are relatively consistent with a general drying pattern across the study region between climate scenarios for the 2020s, but by the 2080s some coastal increase in precipitation is evident (Fig 5.16). The 2080s CGCM3-A2 scenario extends the increase in precipitation to almost the entire study region with some weak decreases in the southern and eastern valley bottoms.

Summer changes to precipitation are projected to be a general decrease in the coastal mountains with a less consistent pattern for the rest of the study region across the scenarios and time periods (Fig 5.17). The largest discrepancy is in the 2080s with a general increase in precipitation for the CGCM3-A2 scenario and a general decrease in precipitation for the HADGEM-A1B scenario for large parts of the study area. The difference between these scenarios is up to 30% of the 1961 – 1990 climate normal.

The autumn precipitation projections are the most consistent between all the seasons and scenarios (Fig 5.18). The models all show an increase in precipitation with extreme values up to 70% during the 2080s for scenario CGCM3-A2. The driest scenario is HADGEM-A1B, which still shows an increase in the 2080s of between 18 and 55%.

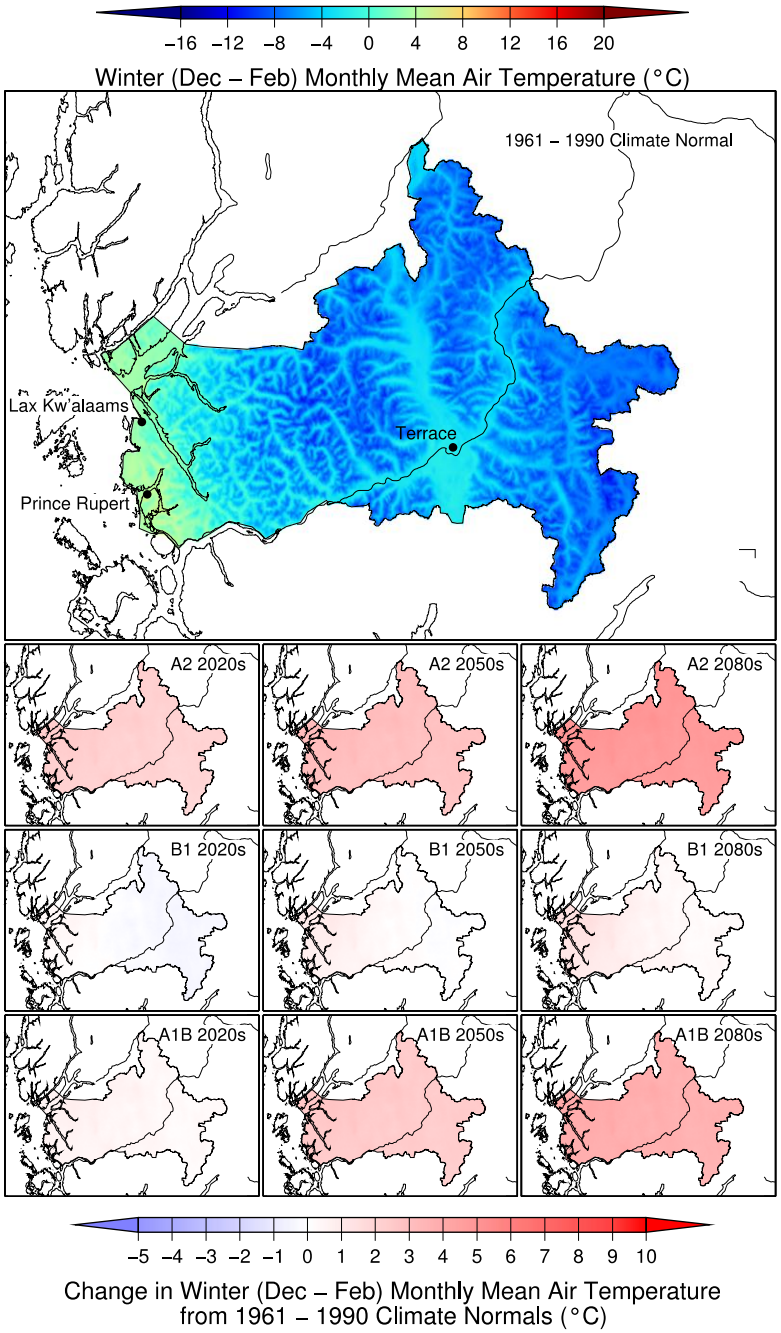

Figure 5.11: Winter monthly mean air temperature for the 1961 – 1990 climate normal (top panel) and changes under each climate scenario for the 2020s (2010-2039), 2050s (2040-2069) and 2080s (2070-2099). The lower three panels represent each emissions/climate scenario's anomaly in order (top to bottom): CGCM3-A2, HADGEM-A1B, and HADCM3-B1, respectively. Anomalies are calculated by subtracting the 1961 – 1990 climate normal (top panel) from a mean climate year created by averaging over 30 years centering on the 2020s, 2050s, and 2080s.

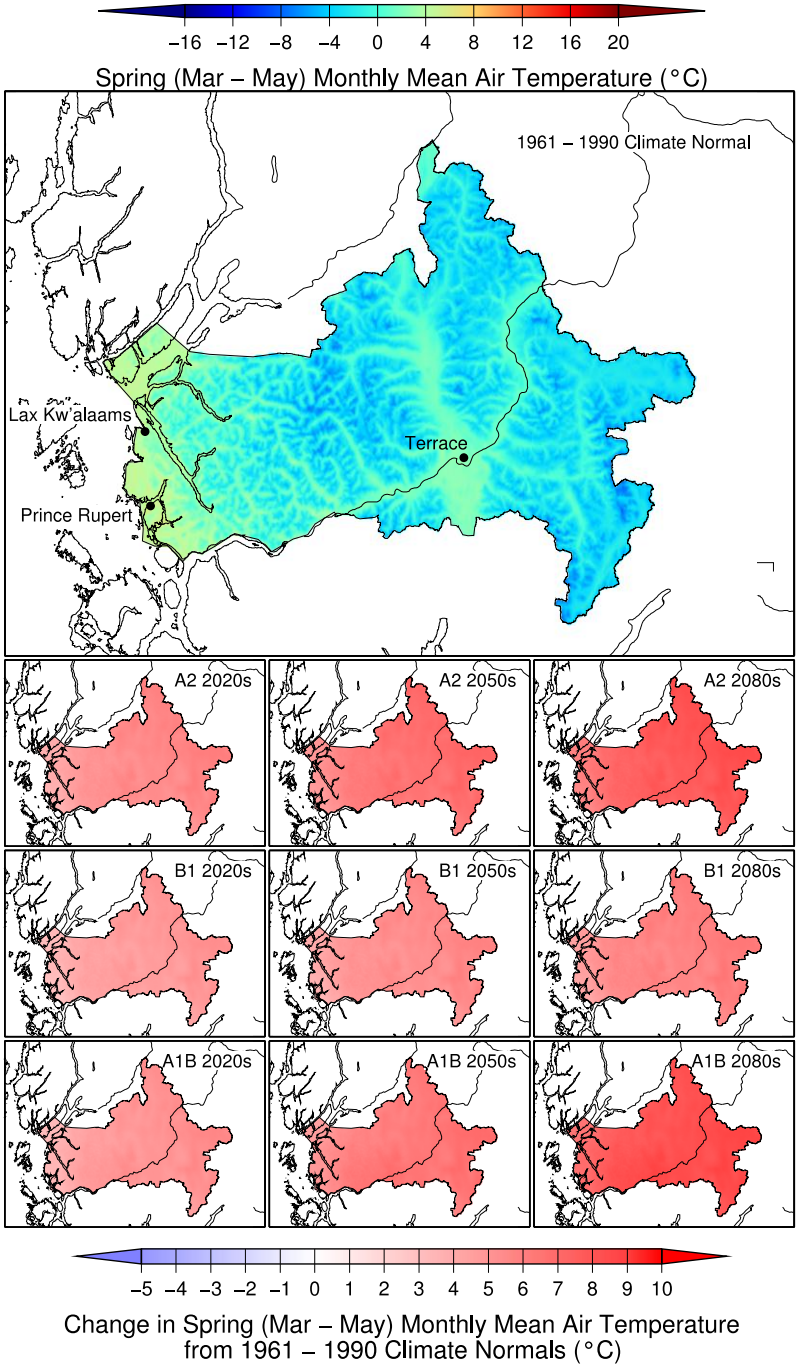

Figure 5.12: Spring monthly mean air temperature for the 1961 – 1990 climate normal (top panel) and changes under each climate scenario for the 2020s (2010-2039), 2050s (2040-2069) and 2080s (2070-2099). The lower three panels represent each emissions/climate scenario's anomaly in order (top to bottom): CGCM3-A2, HADGEM-A1B, and HADCM3-B1, respectively. Anomalies are calculated by subtracting the 1961 – 1990 climate normal (top panel) from a mean climate year created by averaging over 30 years centering on the 2020s, 2050s, and 2080s.

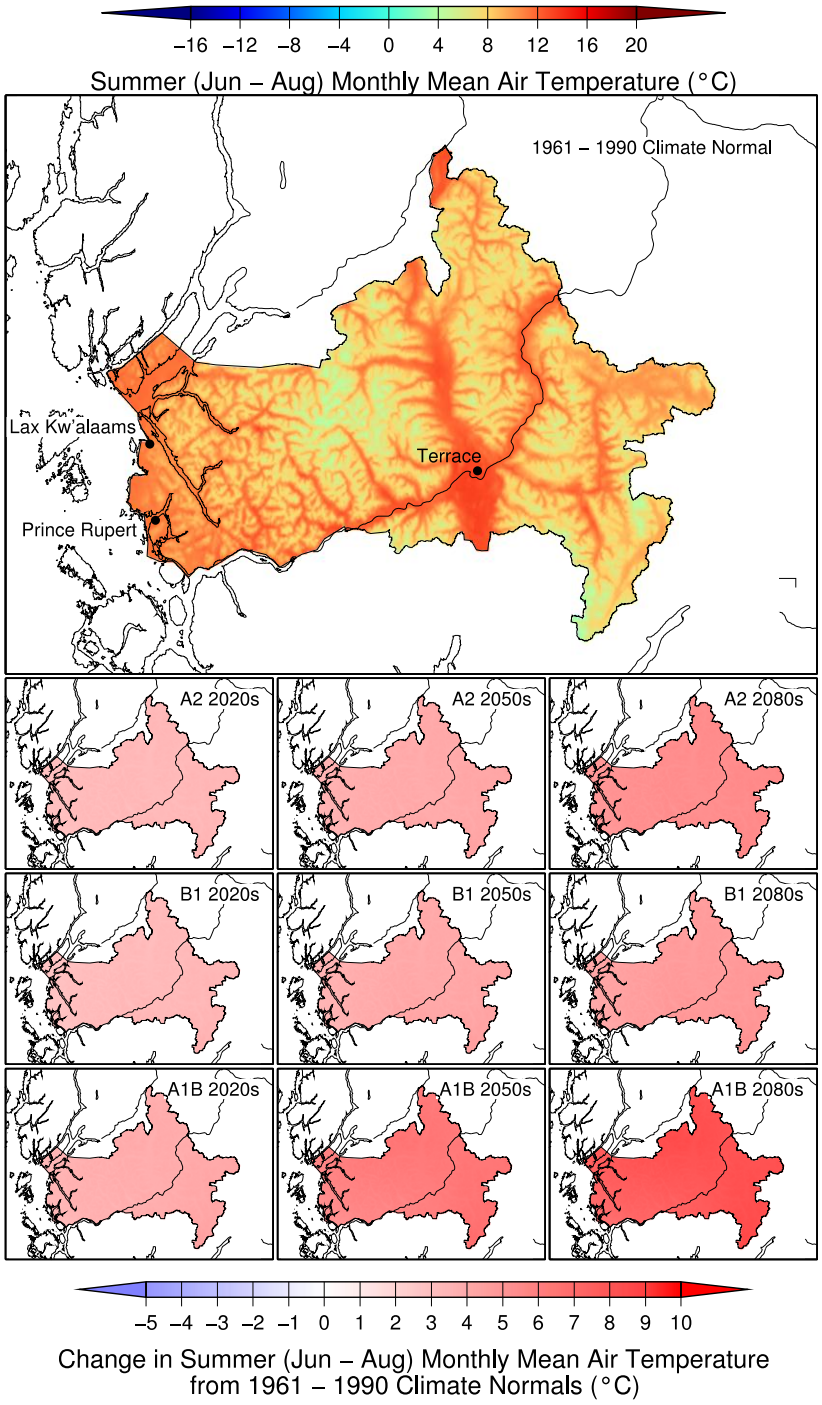

Figure 5.13: Summer monthly mean air temperature for the 1961 – 1990 climate normal (top panel) and changes under each climate scenario for the 2020s (2010-2039), 2050s (2040-2069) and 2080s (2070-2099). The lower three panels represent each emissions/climate scenario's anomaly in order (top to bottom): CGCM3-A2, HADGEM-A1B, and HADCM3-B1, respectively. Anomalies are calculated by subtracting the 1961 – 1990 climate normal (top panel) from a mean climate year created by averaging over 30 years centering on the 2020s, 2050s, and 2080s.

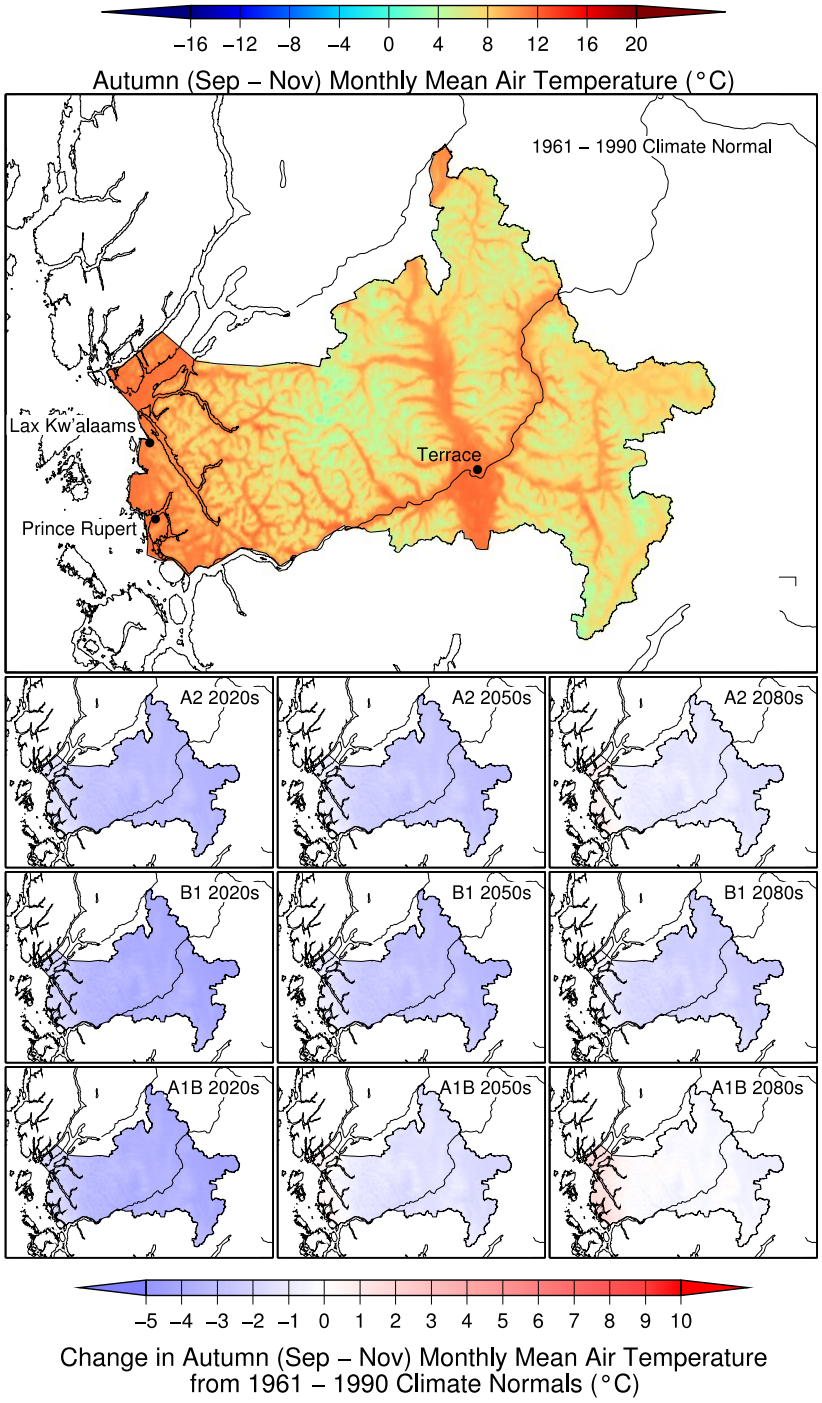

Figure 5.14: Autumn monthly mean air temperature for the 1961 – 1990 climate normal (top panel) and changes under each climate scenario for the 2020s (2010-2039), 2050s (2040-2069) and 2080s (2070-2099). The lower three panels represent each emissions/climate scenario's anomaly in order (top to bottom): CGCM3-A2, HADGEM-A1B, and HADCM3-B1, respectively. Anomalies are calculated by subtracting the 1961 – 1990 climate normal (top panel) from a mean climate year created by averaging over 30 years centering on the 2020s, 2050s, and 2080s.

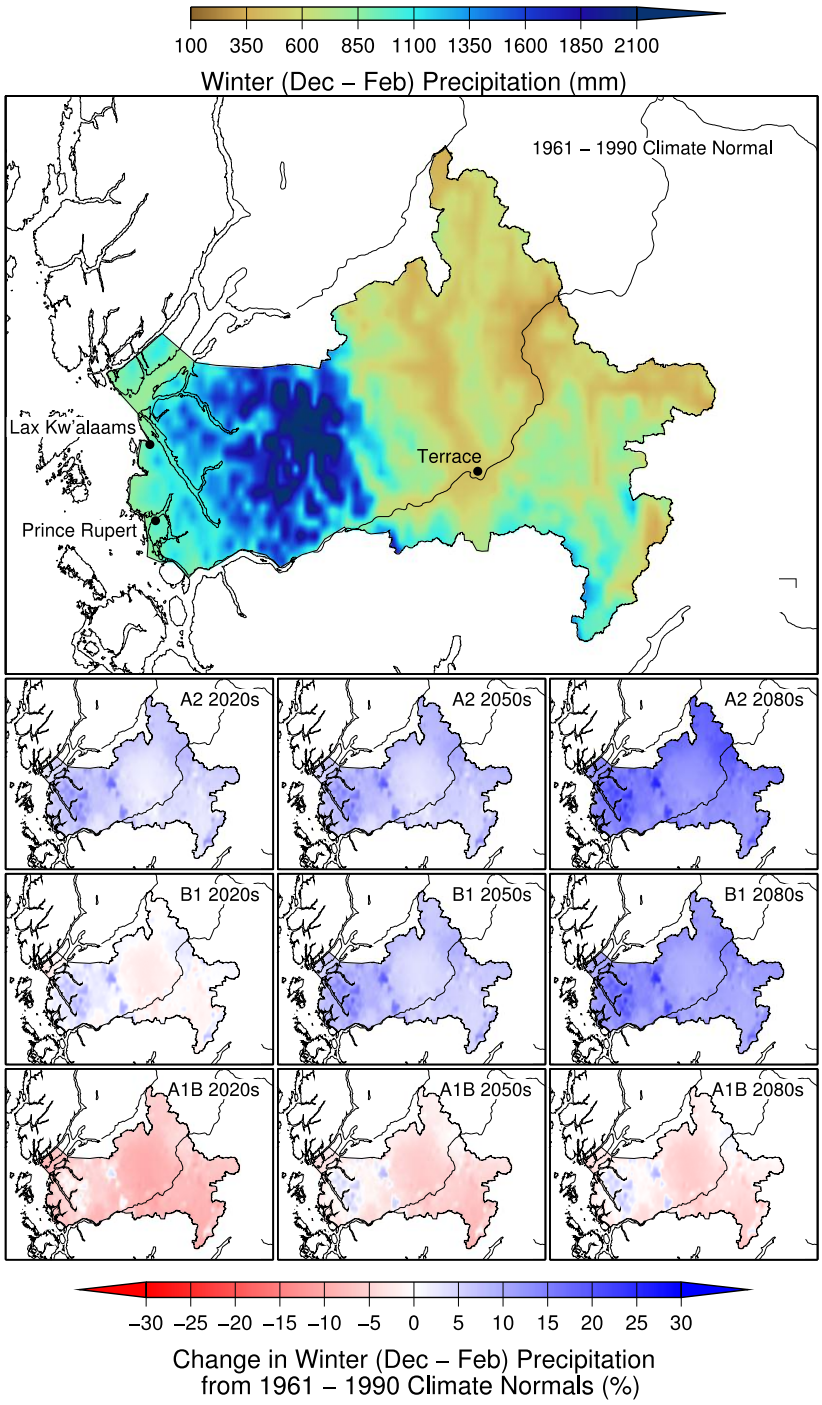

Figure 5.15: Winter precipitation for the 1961 – 1990 climate normal (top panel) and changes under each climate scenario for the 2020s (2010-2039), 2050s (2040-2069) and 2080s (2070-2099). The lower three panels represent each emissions/climate scenario's anomaly in order (top to bottom): CGCM3-A2, HADGEM-A1B, and HADCM3-B1, respectively. Anomalies are calculated by subtracting the 1961 – 1990 climate normal (top panel) from a mean climate year created by averaging over 30 years centering on the 2020s, 2050s, and 2080s. The difference is then presented as a percentage of the 1961 – 1990 climate normal.

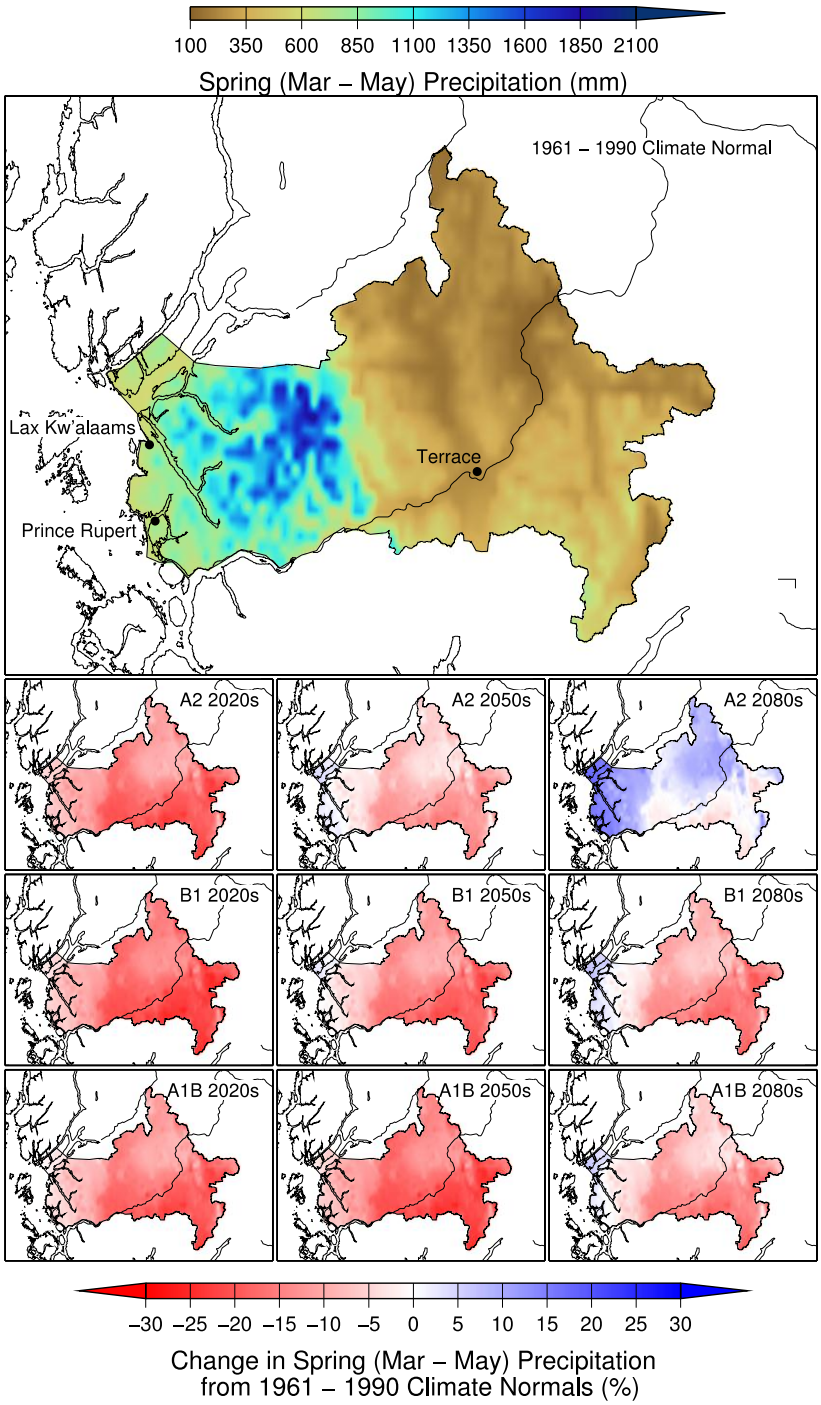

Figure 5.16: Spring precipitation for the 1961 – 1990 climate normal (top panel) and changes under each climate scenario for the 2020s (2010-2039), 2050s (2040-2069) and 2080s (2070-2099). The lower three panels represent each emissions/climate scenario's anomaly in order (top to bottom): CGCM3-A2, HADGEM-A1B, and HADCM3-B1, respectively. Anomalies are calculated by subtracting the 1961 – 1990 climate normal (top panel) from a mean climate year created by averaging over 30 years centering on the 2020s, 2050s, and 2080s. The difference is then presented as a percentage of the 1961 – 1990 climate normal.

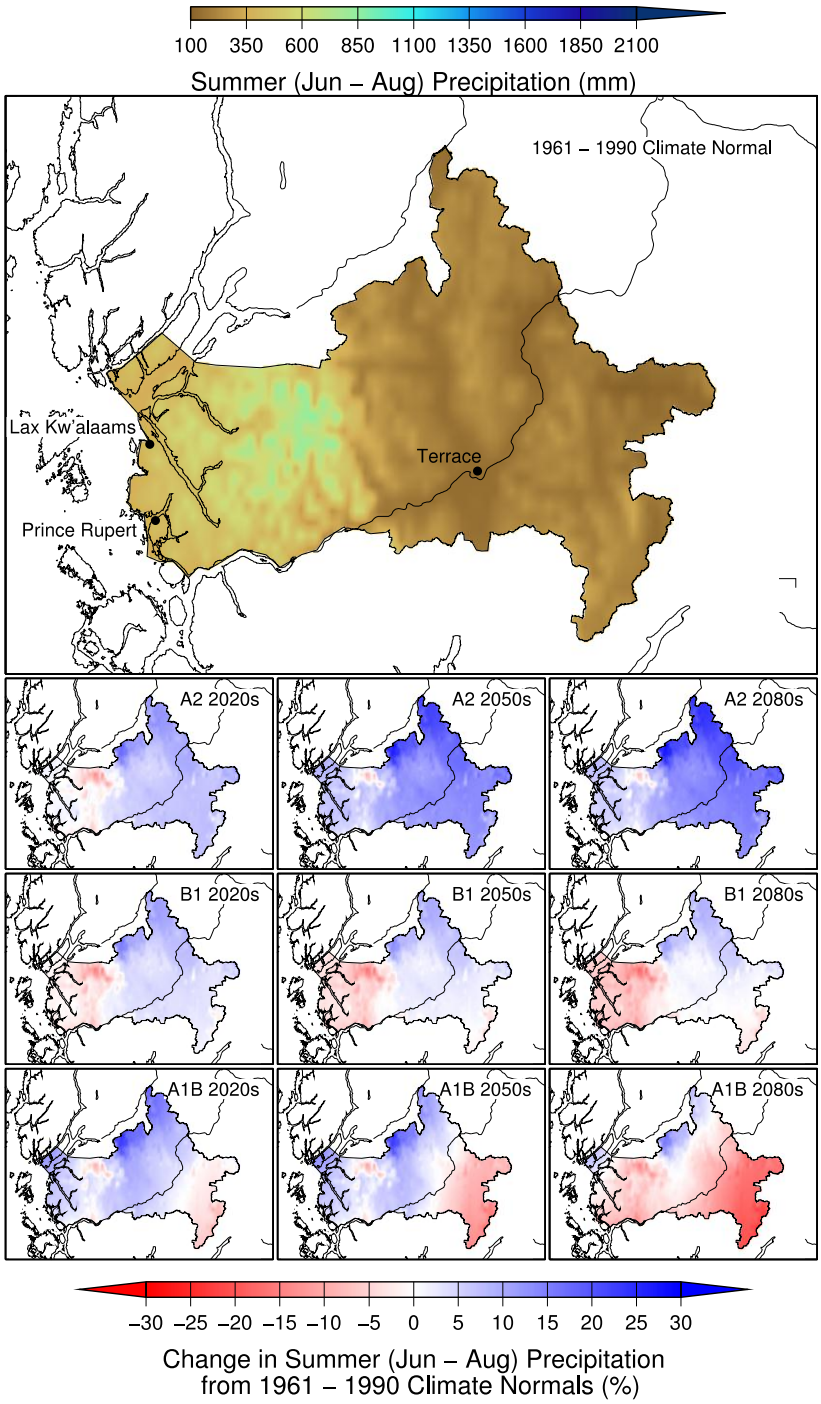

Figure 5.17: Summer precipitation for the 1961 – 1990 climate normal (top panel) and changes under each climate scenario for the 2020s (2010-2039), 2050s (2040-2069) and 2080s (2070-2099). The lower three panels represent each emissions/climate scenario's anomaly in order (top to bottom): CGCM3-A2, HADGEM-A1B, and HADCM3-B1, respectively. Anomalies are calculated by subtracting the 1961 – 1990 climate normal (top panel) from a mean climate year created by averaging over 30 years centering on the 2020s, 2050s, and 2080s. The difference is then presented as a percentage of the 1961 – 1990 climate normal.

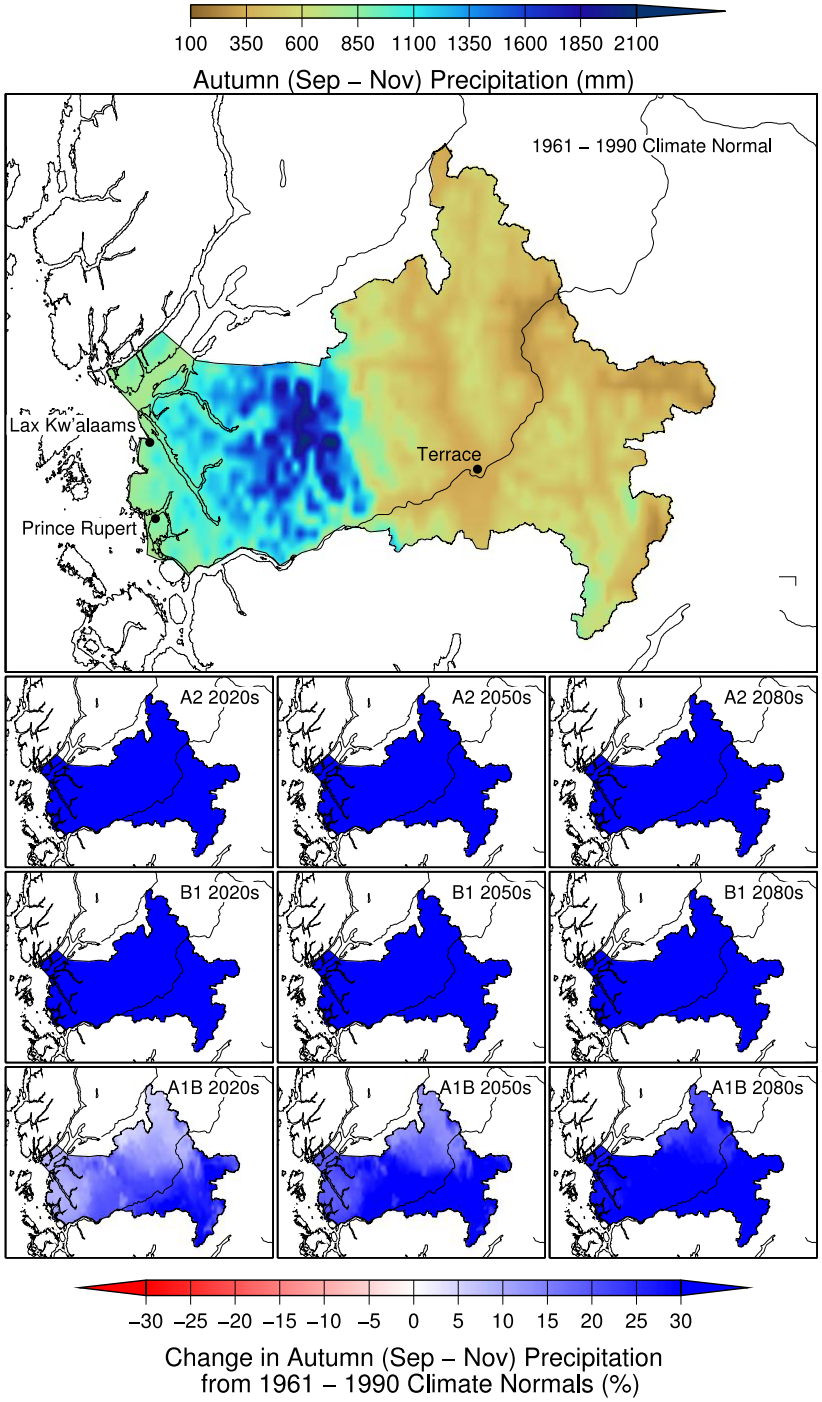

Figure 5.18: Autumn precipitation for the 1961 – 1990 climate normal (top panel) and changes under each climate scenario for the 2020s (2010-2039), 2050s (2040-2069) and 2080s (2070-2099). The lower three panels represent each emissions/climate scenario's anomaly in order (top to bottom): CGCM3-A2, HADGEM-A1B, and HADCM3-B1, respectively. Anomalies are calculated by subtracting the 1961 – 1990 climate normal (top panel) from a mean climate year created by averaging over 30 years centering on the 2020s, 2050s, and 2080s. The difference is then presented as a percentage of the 1961 – 1990 climate normal.

5.3 Literature Survey of Extreme Precipitation and Temperature Changes

Using meteorological records starting from 1950 for Canada, the USA, and Mexico, Peterson et al. (2008) investigated changes in the number of days per year that temperature or precipitation observations were above or below percentile thresholds. They found annual extreme lowest temperatures are warming faster than annual extreme highest temperatures, when the index is assessed as the actual temperature. This trend is suggested to continue in the CGCM2-A2 model outputs (Flato, et al., 2000) described in Sections 5.1.2 and 5.1.3.

Heavy precipitation across North America is also increasing for the average amount of precipitation falling on days of rainfall (thus when there is precipitation, it has higher amounts). These changes have been observed since the late 1960s (Peterson, et al., 2008). The Peterson et al. (2008) observations are supported by a previous study that used only Canadian sites (Bonsal et al., 2001). Bonsal et al. (2001) found, for the majority of southern Canada, a trend of decreasing numbers of days with extreme low temperature during winter, spring and summer, and an increasing trend in the number of days with extreme high temperature in spring and winter. The number of extreme hot summer days was not seen to change significantly. However, these differences are strongly muted around the coastal regions of B.C. with much of the differences in annual extremes of daily maximum temperature between time periods of 1900 – 1949 and 1950 – 1998 dropping to near zero at the coast. There does, however, remain a strong decrease in the heating degree-days at the Prince Rupert meteorological station (heating degree days are a measure intended to reflect the demand for energy required to heat a home or business).
From the Environment Canada meteorological records available for Prince Rupert and Terrace (See Chapter 1.5 and Appendices 1.4 and 1.5), warming trends are evident in both extreme minimum winter temperature and extreme summer warm temperatures (See Chapter 1.5 and Appendices 1.4 and 1.5). Extreme precipitation events are not included in the monthly meteorology used in generation of this report.

Future western North America projections from an ensemble of 19 climate models (Meehl, et al., 2007) suggest a decrease in temperature variability for the winter months. However, the models also project an increase in monthly mean precipitation variability both in absolute and relative amounts.

Using an ensemble of regional climate models, covering the western United States and part of B.C. ending just north of the northern tip of Vancouver Island, Leung et al. (2004) find an increase in precipitation extremes during the cold season by up to 10% for 2040 to 2060. For the A2 emissions scenario, Diffenbaugh et al. (2005) simulated the entire USA and a small area of southern Canada (most northern extent is the northern tip of Vancouver Island). They project widespread, significant increases in extreme precipitation events, particularly on the lee side of rain shadows.

5.4 Literature Survey of Extreme and Mean Wind Speed

Several studies have looked at wind speeds in the Pacific Northwest and B.C. Many of these studies have conflicting conclusions regarding changes in historical extreme and mean wind speeds. A recent study, focusing on three locations in the inner south coast of B.C. (48° – 49° N, 123° W),

investigated wind speeds in response to climate variability (Abeysirigunawardena et al., 2009). Their analysis indicated an important relationship between local extreme wind speeds and the phases of the El Niño Southern Oscillation (ENSO), a periodic climate-ocean pattern that occurs over the tropical Pacific and influences climate on an almost-global scale. Higher extreme winds speeds corresponded to negative (cold La Niña) ENSO phases during the observational period of 1953 – 2006 (with only single meteorological station coverage for the first 40 years of the record).

Griffin et al. (2010) investigated the Pacific Northwest region from 45° to 51°N using data from 92 meteorological stations. They found a different trend for coastal versus more inland sites with coastal sites experiencing an eight to nine year cyclic pattern and more inland sites showing a small linear downward trend in wind speed through time. Stronger winds and greater variability are also more common at coastal sites than further inland. Future changes to extreme wind events has been discussed by the IPCC (2007):

> A number of modeling studies have also projected a general tendency for more intense but fewer storms outside the tropics, with a tendency towards more extreme wind events and higher ocean waves in several regions in association with those deepened cyclones. Models also project a poleward shift of storm tracks in both hemispheres by several degrees of latitude. (Meehl, et al., 2007, p. 783)

While this implies an increase in extreme wind speeds, with a decrease in the number of storm events, the spatial scale covered by this IPCC statement is very large and thus possibly not directly applicable for our study region.

5.5 Climate Summary and Future Projections

The climate of the Skeena region will likely warm significantly and become wetter into the future. This warming will be felt across most seasons with a possible cooling in the autumn months. Precipitation patterns will likely shift to drier spring months with much wetter autumn months. The actual magnitude of the changes in temperature and precipitation are highly dependent upon emissions/model scenarios. Extreme precipitation events are likely to increase, primarily in the cold season months. Extreme minimum and maximum temperatures are also likely to increase into the future. Variability of the climate is thus likely to increase into the future. Evidence from ecosystem studies suggests that this enhanced variability could have stronger impacts upon the ecosystems of the study region than any of the overall trends and shifts in annual values (Jentsch et al., 2008).

Table 5.4: Future projections for climate with an estimated confidence level. For a calibration of the projection confidence level please see Appendix 6.1.6.

Parameter	Source of estimation	Likely Direction of Change	Projection Confidence Level* (see Appendix 6.1.6)	Comments
Mean annual temperature	IPCC climate models result for FFESC study area	Increase (warming)	High	Demonstrated in all three climate models/scenarios. Actual magnitude of the increase is variable between scenarios/climate models, also dependent upon proximity to the coast.
Total annual precipitation	IPCC climate model result for FFESC study area	Increase (wetter)	Moderate	Strong increase in two of three climate models/scenarios. Over 20% increase compared to present day dependent upon scenario/ climate model and location within study region. Climate model / scenario HADGEM-A1B shows only a small increase.
Extreme low temperature values annual and seasonal	Regional meteorological records and scientific literature	Increase (warming)	Moderate	See Section 5.2.3. Evident both historically and in future projections.
Extreme high temperature values annual and seasonal	Regional meteorological records and scientific literature	Increase (warming)	Moderate	See Section 5.2.2. Evident both historically and in future projections.
Extreme and mean wind speed	Scientific literature	Uncertain	Very Low / None	See Section 5.4

References:

Abeysirigunawardena, D. S., Gilleland, E., Bronaugh, D., & Wong, P. (2009). Extreme wind regime responses to climate variability and change in the inner south coast of British Columbia, Canada. Atmosphere-Ocean, 47(1), 41-62. doi: 10.3137/Ao1003.2009

Bonsal, B. R., Zhang, X., Vincent, L. A., & Hogg, W. D. (2001). Characteristics of daily and extreme temperatures over Canada. Journal of Climate, 14(9), 1959-1976.

Cohen, S. J., & Waddell, M. W. (2009). Climate Change in the 21st Century. Montreal & Kingston: McGill-Queen's University Press.

Diffenbaugh, N. S., Pal, J. S., Trapp, R. J., & Giorgi, F. (2005). Fine-scale processes regulate the response of extreme events to global climate change. Proceedings of the National Academy of Sciences of the United States of America, 102(44), 15774-15778. doi: 10.1073/Pnas.0506042102

Flato, G. M., Boer, G. J., Lee, W. G., McFarlane, N. A., Ramsden, D., Reader, M. C., & Weaver, A. J. (2000). The Canadian Centre for Climate Modelling and Analysis global coupled model and its climate. Climate Dynamics, 16(6), 451-467.

Griffin, B. J., Kohfeld, K. E., Cooper, A. B., & Boenisch, G. (2010). Importance of location for describing typical and extreme wind speed behavior. Geophysical Research Letters, 37. doi: 10.1029/2010gl045052.

Jentsch, A., & Beierkuhnlein, C. (2008). Research frontiers in climate change: Effects of extreme meteorological events on ecosystems. Comptes Rendus Geoscience, 340(9-10), 621-628. doi: 10.1016/J.Crte.2008.07.002

IPCC. (2001). Climate change 2001: The scientific basis. Contributions of Working Group I to the Third Assessment Report of the Intergovernmental Panel on Climate Change. In J. T. Houghton, Y. Ding, D. J. Griggs, M. Noguer, P. J. v. d. Linden, X. Dai, K. Maskell & C. A. Johnson (Eds.), (pp. 881). Cambridge, U.K. and New York USA.

Leung, L. R., Qian, Y., Bian, X. D., Washington, W. M., Han, J. G., & Roads, J. O. (2004). Mid-century ensemble regional climate change scenarios for the western United States. Climatic Change, 62(1-3), 75-113.

Manning, M. R., Edmonds, J., Emori, S., Grubler, A., Hibbard, K., Joos, F., van Vuuren, D. P. (2010). Misrepresentation of the IPCC CO_2 emission scenarios. Nature Geoscience, 3(6), 376-377.

Meehl, G. A., & Stocker, T. F., W.D. Collins, P. Friedlingstein, A.T. Gaye, J.M. Gregory, A. Kitoh, R. Knutti, J.M. Murphy, A. Noda, S.C.B. Raper, I.G. Watterson, A.J. Weaver, Z.-C. Zhao (Eds.). (2007). Global Climate Projections. Cambridge, United Kingdom and New York, USA: Cambridge University Press.

Nakicenovic, N., Alcamo, J., Davis, G., Vries, B. d., Fenhann, J., Gaffin, S., . . . Dadi, Z. (Eds.). (2000). IPCC Special Report on Emissions Scenarios. Cambridge, UK: Cambridge University Press.

Peterson, T. C., Zhang, X. B., Brunet-India, M., & Vazquez-Aguirre, J. L. (2008). Changes in North American extremes derived from daily weather data. Journal of Geophysical Research-Atmospheres, 113(D7). doi: 10.1029/2007jd009453

Spittlehouse, D., & Murdock, T. (2010). Choosing and applying climate change scenarios. Draft. FFESC Project 014. Victoria, B.C.

Wang, T., Hamann, A., Spittlehouse, D. L., & Aitken, S. N. (2006). Development of scale-free climate data for western Canada for use in resource management. International Journal of Climatology, 26(3), 383-397.